ADVANCED MATERIALS
www.advmat.de

Atomic Layer Deposition on Dispersed Materials in Liquid Phase by Stoichiometrically Limited Injections

*Benjamin P. Le Monnier, Frederick Wells, Farzaneh Talebkeikhah, and Jeremy S. Luterbacher**

Atomic layer deposition (ALD) is a well-established vapor-phase technique for depositing thin films with high conformality and atomically precise control over thickness. Its industrial development has been largely confined to wafers and low-surface-area materials because deposition on high-surface-area materials and powders remains extremely challenging. Challenges with such materials include long deposition times, extensive purging cycles, and requirements for large excesses of precursors and expensive low-pressure equipment. Here, a simple solution-phase deposition process based on subsequent injections of stoichiometric quantities of precursor is performed using common laboratory synthesis equipment. Precisely measured precursor stoichiometries avoid any unwanted reactions in solution and ensure layer-by-layer growth with the same precision as gas-phase ALD, without any excess precursor or purging required. Identical coating qualities are achieved when comparing this technique to Al_2O_3 deposition by fluidized-bed reactor ALD (FBR-ALD). The process is easily scaled up to coat >150 g of material using the same inexpensive laboratory glassware without any loss in coating quality. This technique is extended to sulfides and phosphates and can achieve coatings that are not possible using classic gas-phase ALD, including the deposition of phosphates with inexpensive but nonvolatile phosphoric acid.

Atomic layer deposition is a layer-by-layer deposition technique that relies on two half reactions that occur between a vapor phase and a solid substrate. The first reaction involves precursor exposure followed by purging with an inert gas to remove the excess of reactant. Second, the substrate is exposed to a counter-reactant also followed by a purge cycle. The key feature of this process is that both surface reactions with the precursor and counter-reactant are self-limited, which prevents deposition of more than an atomic monolayer per full cycle.[1] During this process, the reactor is typically maintained below atmospheric pressure within a temperature window that allows vaporization of the reactants without thermal decomposition.

Elemental zinc and elemental sulfur were the first precursor and counter-reactant, respectively, used for ZnS atomic layer deposition.[2] Since then, processes for depositing a range of materials including oxides, nitrides, hybrids and even metals have been developed.[3–5] This wide variety of materials combined with its atomic-level precision has made ALD a formidable tool for the fabrication of nanostructured materials such as transistors, solar cells and fuel cells.[6]

More recently, processes have been developed to apply ALD to high-surface-area materials (>10 m^2 g^{-1}), including powders for various applications, from passivation of photoactive material to catalyst preparation.[7,8] With such materials, long exposure time (minutes vs milliseconds for wafers), both for purge and reaction cycles, must be coupled with effective dispersion techniques to overcome mass transfer limitations. Setups typically include rotating reaction chambers or fluidized beds to disperse the particles, and will require extensive precursor recycling schemes at the industrial scale. The complexity of these installations has limited the application of this technique in research and, up to now, prevented its industrial implementation despite exciting published results.[9,10]

In this context, new strategies using deposition in liquid phase are emerging. Notably, we have used continuous injection of sol gel precursors to deposit reasonably conformal but systematically porous coatings.[11,12] Other work has focused on subsequent liquid-phase injections of ALD or sol gel precursors, but the coating quality was systematically much less conformal than that obtained with gas-phase ALD, likely because they involved oligomerization-precipitation mechanisms.[13–15] Other self-limited layer-by-layer liquid phase deposition processes such as successive ionic layer adsorption and reaction (SILAR) or microfluidic ALD on plates have been developed,[16,17] but, like gas-phase ALD, they use huge precursor (and solvent) excesses and cannot be used to coat dispersed substrates like powders. Liquids could greatly facilitate deposition on dispersed high-surface-area substrates such as powders due to their higher density and viscosity compared to gas, which can effectively disperse these nanostructured materials without extensive mixing or fluidization.

Here, we designed an ALD procedure requiring only common inorganic chemistry laboratory equipment that avoids any excess of precursors and is simple to scale up, all while

B. P. Le Monnier, F. Wells, F. Talebkeikhah, Prof. J. S. Luterbacher
Laboratory of Sustainable and Catalytic Processing
Institute of Chemical Sciences and Engineering
École Polytechnique Fédérale de Lausanne (EPFL)
CH-1015 Lausanne, Switzerland
E-mail: jeremy.luterbacher@epfl.ch

The ORCID identification number(s) for the author(s) of this article can be found under https://doi.org/10.1002/adma.201904276.

DOI: 10.1002/adma.201904276

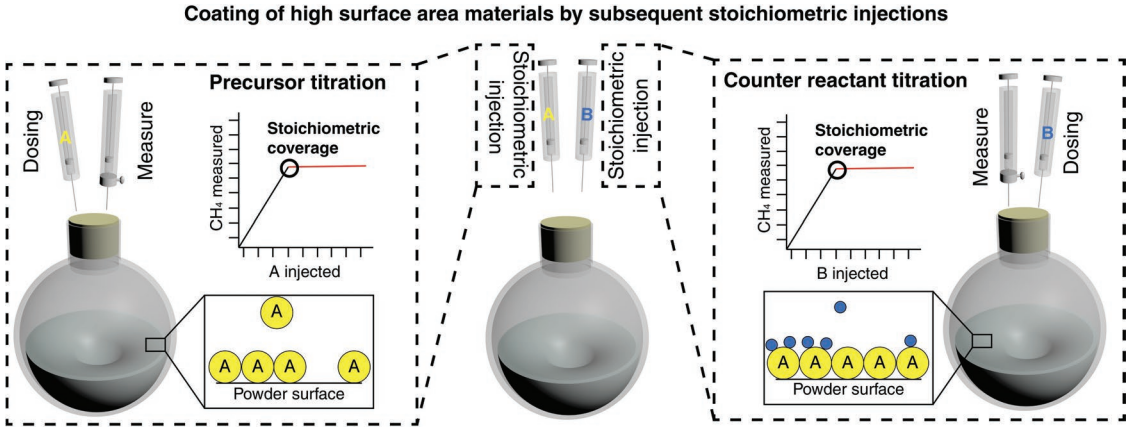

Figure 1. Process of the liquid phase ALD by stoichiometric injection based on precursor and counter-reactant titration of dispersed powder substrate.

achieving similar coating qualities to gas-phase ALD. The basic principle (**Figure 1**) involves the dispersion of the powder substrate in a solvent and determination of the exact quantities of reactants to inject by titration of the precursor (and counter-reactant) prior to deposition, which is crucial to ensure high-quality coatings. Therefore, the deposition can be performed in a simple round-bottom flask at room temperature and pressure.

We extensively studied alumina growth on silica using trimethyl aluminum (TMA) and water as the precursor and counter-reactant, as it was a well-studied system in gas-phase ALD[18] and we could also rely on work involving the grafting of alkyl aluminum in liquid phase on silica.[19,20] Nevertheless, we tested and showed that the approach is compatible with precursors releasing a nonvolatile side like tri-octyl aluminum (see Section S3 in the Supporting Information).

In our procedure, we first have to titrate the surface with the precursor, and then titrate a precursor-saturated surface with the counter-reactant. In both cases, the reactions between the precursor or counter-reactant are followed by the release of methane (**Figure 2**). The injected TMA reacted with surface hydroxyl groups on the dispersed catalyst and released methane (Figure 2a). A remarkable benefit of this titration approach is that it allows for the in situ monitoring of surface reactions and provides insight into the nature of these reactions. The slope of the methane released versus TMA added reveals the number of methane atoms released per aluminum (Figure 2a,b). Because the reaction is self-limiting, once the surface is saturated with TMA, a slope close to zero is observed as no more reaction occurs (Figure 2a). Depending on the hydroxyl group density, each TMA molecule can react once or more with the surface, forming pending or bridging aluminum surface species (Figure 2b).[21]

Once the saturation point of TMA is established, a batch of catalyst could be covered with exactly one monolayer of aluminum in order to perform the water titration on the aluminum-covered surface. Similarly, water was added and the methane release was monitored (Figure 2c). Different slopes were observed depending on the reactions involved, which include the formation of a pending hydroxyl group or of an oxo bridge (Figure 2d).[22] Two separate regimes were observed in one titration (Figure 2c). In such cases, when water was injected, it appeared to react more favorably with dense populations of adsorption sites by forming bridges, leading to the release of two methane molecules (slope of 2). Following the consumption of dense sites, water reacted with the remaining isolated sites, releasing one molecule of methane per molecule of water (slope of 1). A similar effect was previously suggested by McCormick et al., when using a rotary ALD reactor.[23] These results are highly analogous to plots showing growth rate versus pulse time in ALD studies, which demonstrates the self-limited deposition of both reactants on the surface.[24,25] The closed methane balance at each cycle confirmed the accuracy of each subsequent titration (Figure S1, Supporting Information).

The growth per cycle (GPC) for both aluminum and water was determined by dosing the amount of aluminum and water required to saturate each layer. When starting with a silica surface with a low density of hydroxyl groups (Figure 2e), the quantity of aluminum grafted at each cycle kept increasing. This phenomenon is known in the ALD literature as being characteristic of a nucleation growth.[26] Isolated hydroxyl groups on the silica surface are the seeds for nucleation, from which each particle grows from cycle to cycle. We can measure, at each cycle, an average number of aluminum atoms per cluster on dispersed silica by simply using gas chromatography. Interestingly, the water-to-aluminum ratio alternates between 1.1 ± 0.1 and 1.6 ± 0.2, which suggests that the alternate formation of mostly bridge (ratio of 1) or a mixture of bridge and pending (ratio of 2) functional groups. This sequence can be explained by a simple model (Figure 2f). When a substrate is covered with a low density of individual hydroxyl groups, adsorbed aluminum will be mostly mono-grafted, and two water molecules are then required to hydrolyze the two pending methyl group on each aluminum (high water-to-aluminum ratio). As a consequence, the next layer is made of a denser layer of available hydroxyl groups, favoring the formation of a large majority of bridging aluminum, leading to a water-to-aluminum ratio of close to 1.

When starting with silica that contained a higher density of OH groups and a bit of physisorbed water (8 OH per nm^2, Figure 2g), the aluminum GPC initially increased but stabilized after the 4th cycle. As opposed to nucleation growth, a stable GPC is indicative of a relatively flat film growth, as each added layer contains the same quantity of aluminum. To inject the exact quantities of precursor to achieve one monolayer of coverage, we repeated our reactant and counteractant titration

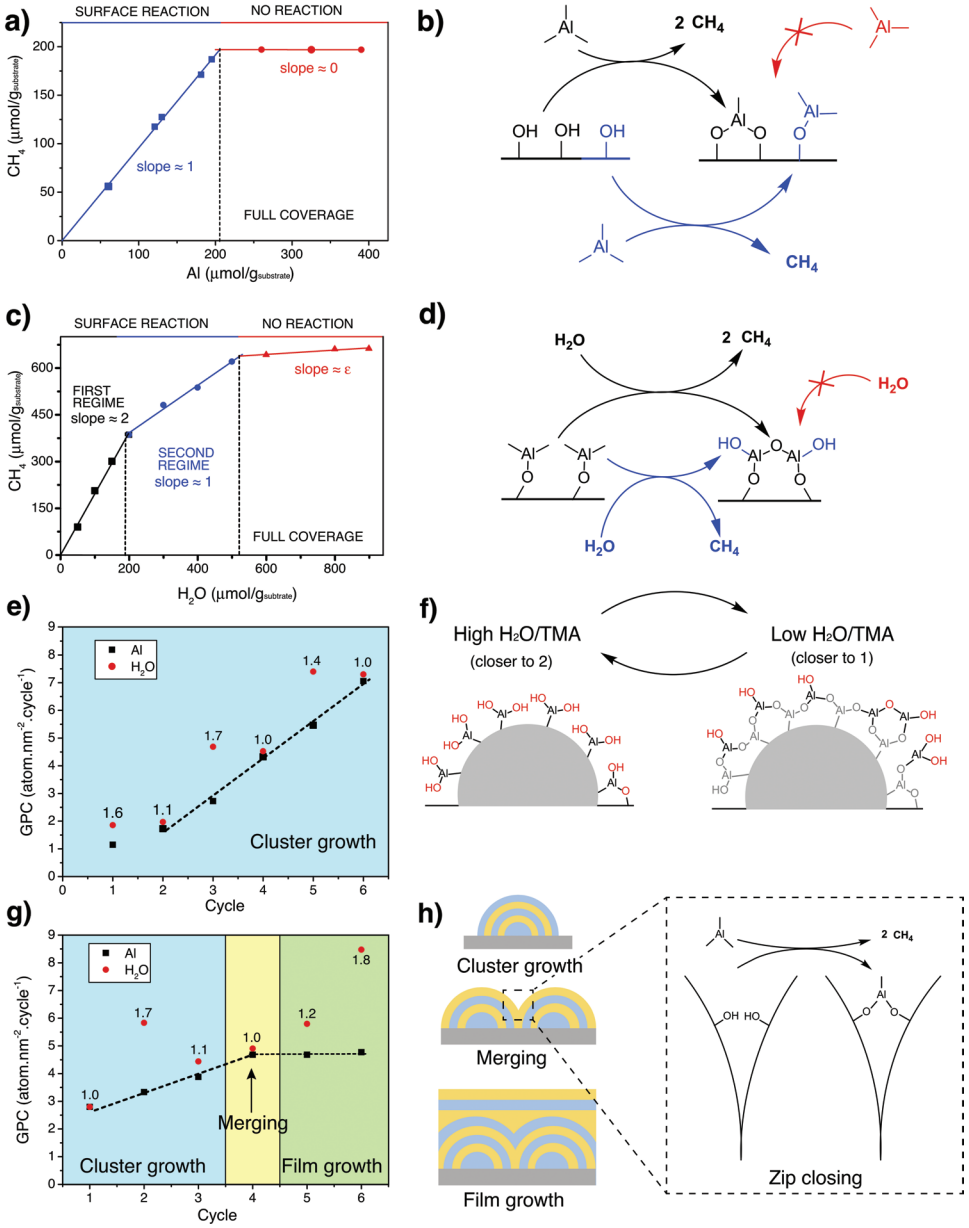

Figure 2. Surface titration by released methane quantification and mechanisms of alumina growth. a) Surface titration of available hydroxyl groups during TMA addition normalized by initial mass of substrate. b) Reaction schemes for TMA and a hydroxylated surface leading to the release of one or two molecules of methane per TMA. c) Surface titration of hydrolyzable methyl groups after deposition of a stoichiometric quantity of TMA. d) Reaction schemes for water and an alkyl aluminum-covered surface leading to the release of one or two molecules of methane per molecule of water. e,g) Growth per cycle (GPC), (i.e., quantity added at saturation) determined by TMA and water surface titration at each cycle on silica nanospheres, normalized by surface area with a starting hydroxyl density of: e) 2 OH nm^{-2} and g) 8 OH nm^{-2}. The numerical labels above the water points refer to the water/aluminum ratio. f) Schematic representation of cluster growth showing, alternatively, a surface covered by pending aluminum, or bridging aluminum, leading to alternating high (up to 2) and low (as low as 1) water-to-aluminum ratios during each cycle. h) Sketches illustrating the various steps of ALD growth that were observed: the nucleation and growth of clusters, their merging, and continuous film growth.

at each cycle until the film growth phase was achieved. During film growth, the ratio of water to aluminum that is grafted still alternated between high and low as this does not depend on the shape of the previous layer (which was also observed for high surface silica, see Figure S2, Supporting Information). The regime between nucleation and continuous film growth is characteristic of merging nuclei, which features a notable increase in bridging oxygens as two nuclei merge (Figure 2h).

A series of materials was prepared by performing several cycles with saturating quantities of TMA and water as measured by the results of the aforementioned titrations (**Figure 3**), using a round-bottom flask under a fumehood (Figure S3, Supporting Information). Silica nanospheres were coated with 10 TMA/water cycles in order to clearly assess the overcoating density and conformality (Figure 3a–c). As a benchmark, we performed a conventional gas-phase ALD coating in a fluidized

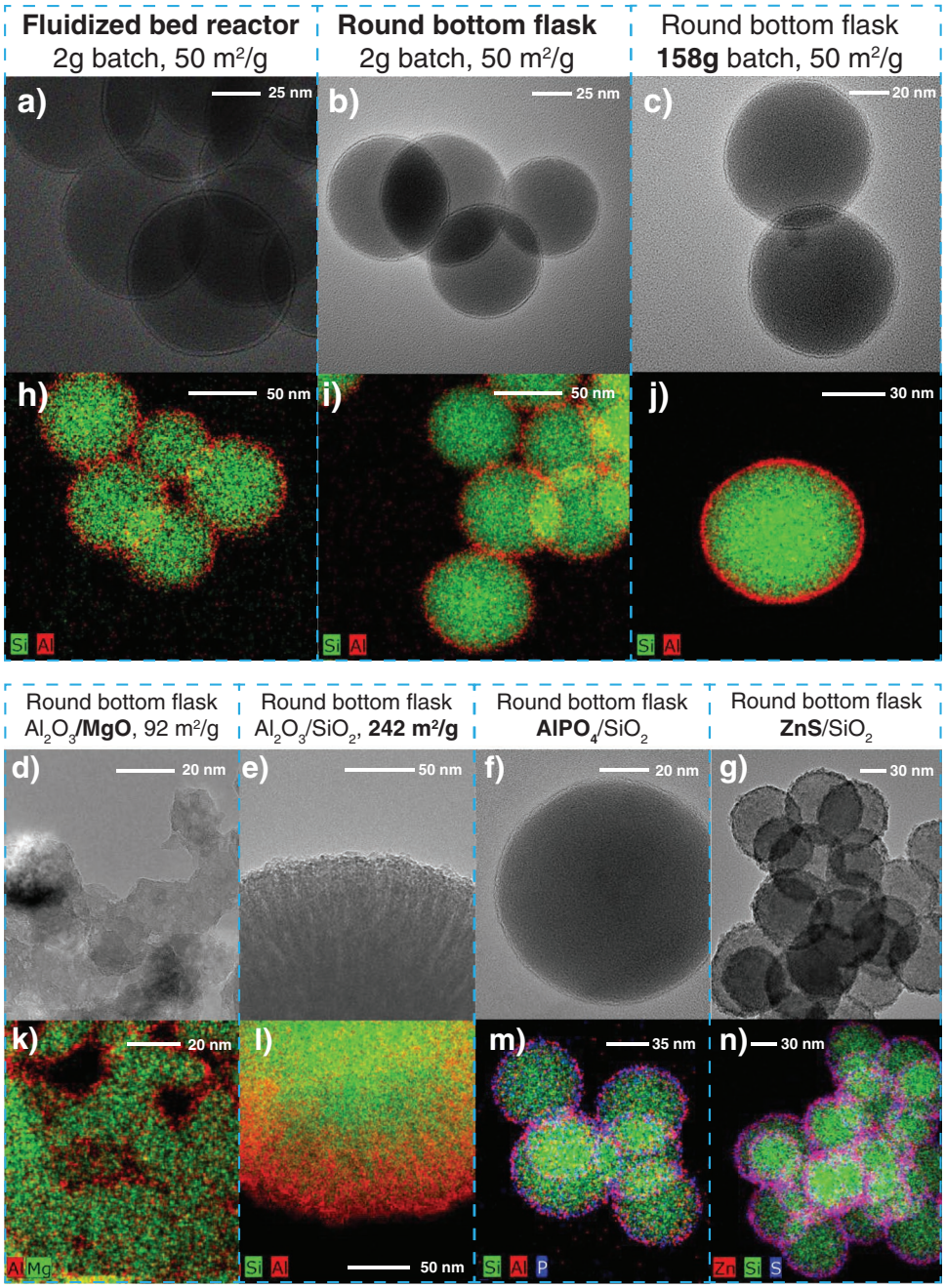

Figure 3. a–c) Bright-field transmission electron microscopy images of silica spheres coated with 10 cycles of TMA/water deposition using: a) a commercial fluidized bed reactor ALD (2 g batch), b) a round bottom flask (2 g batch), and c) the same procedure up-scaled to 158 g. d) The same deposition method but on a basic substrate (MgO) with slightly higher surface area and e) using a high-surface-area silica as a substrate. f) $AlPO_4$ deposited onto silica particles using the same method but replacing H_2O by H_3PO_4 as a counter-reactant. g) ZnS deposited onto silica spheres by the same liquid phase method using diethyl zinc and hydrogen sulfide as reactants. h–n) Elemental mapping of the corresponding coated samples above using scanning transmission electron microscopy with an energy-disperse X-ray detector.

bed reactor (FBR) at 140 °C under reduced pressure (<1 torr) (Figure 3a). The coating quality and conformality were identical with no uncoated or partially coated particles being observed in either case. We always observed an absence of agglomeration and did not observe any alumina on the surface (additional images comparing the methods are shown in Figure S4 in the Supporting Information). Interestingly, the layer deposited in solution was actually thinner (1.5 nm vs 3 nm) and closer to what would be expected for ten monolayers of alumina (≈1 nm) deposited by TMA/H_2O cycles.[15] The thicker layer in FBR-ALD could be indicative of a CVD growth mechanism occurring in the FBR where the water was likely not fully desorbed between the cycles at 140 °C.[27] The two materials were also compared by solid-state NMR, X-ray diffraction (XRD), and X-ray

photoemission spectroscopy (XPS) (Figures S5–S7, Supporting Information). These chemical and structural analyses confirmed that, in both cases, amorphous alumina was present and that the aluminum was in the same chemical environment.

Importantly, scaling up the coating procedure using our method was simple and inexpensive. We prepared a batch of 158 g of coated silica, using the same conditions with a bigger round-bottom flask and more concentrated injections. The quality of the coating was completely unaffected (Figure 3c) and no unattached aluminum or agglomeration was observed by STEM-EDX (Figure 3h–j). The stoichiometrically limited method can be applied to numerous materials, both for coatings and supports. We used the same approach applied for alumina growth on silica to coat higher surface area and basic material such as magnesia (Figure 3d and Figure S8, Supporting Information) with alumina.

The aforementioned materials were prepared by injections separated by 30 min, without any purging or drying steps. After further optimization, we were able to reduce the time between injections to 10 min while maintaining coating quality (Figure S9, Supporting Information). The material prepared by FBR-ALD followed this sequence: TMA injection (4 min), purge (40 min), water injection (4 min), and purge (40 min). The optimal FBR-ALD sequence can depend on the setup, but in our case, shorter injection times led to incomplete coverage. This sequence corresponds to a huge excess of precursor and large amounts of purging gas. In contrast, stoichiometric injections, regardless of the time between injections, use no excess of precursor, which could tremendously reduce ALD processing costs. The disadvantage of the method presented here is that it does require an initial sacrificial titration run to characterize the quantities required for injection. However, this would quickly become worthwhile for a large batch of precursor. Gas-phase ALD coatings on wafers are significantly shorter (<1 s per cycle) and thus are much easier to scale up compared to gas-phase ALD on high-surface-area substrates.

To further demonstrate the versatility of our method, a high-surface-area silica (KCC-1) that is typically used in heterogeneous catalysis was also coated with 10 cycles of TMA/water. STEM-EDX mapping (Figure 3l; Figure S10, Supporting Information) confirmed the deposition of alumina within pores, and once again no freestanding alumina was detected. N_2 physisorption analysis (Figure S11, Supporting Information) showed an expected decrease of the BET surface area from 356 to 242 $m^2\ g^{-1}$ due to the reduction in pore size, but also a preservation of some micro- and mesoporosity. The remaining porosity confirmed that the deposition did not simply occur on the outer shell and did not clog pores, which could negatively affect catalysis.

We also wanted to demonstrate that certain coatings that cannot be achieved in the gas phase can be done using liquid-phase stoichiometrically limited injections. One such example is the deposition of phosphates including aluminum phosphates. This can be done in conventional ALD, but requires six steps with three reactants to perform self-limited reactions, including more expensive sources of phosphorus such as trimethylphosphate or triethylphosphate.[28–30]

Phosphate deposition in gas phase is challenging due to the low volatility of many phosphate precursors. Sol–gel approaches are easier but do not provide the same degree of accuracy.[30] Here, we were able to deposit high-quality aluminum phosphate coatings on silica using our conventional two injections with TMA and inexpensive phosphoric acid (Figure 3f,m; Figure S12, Supporting Information). The phosphate structure was confirmed by solid-state aluminum and phosphorous NMR as well as by XPS (Figures S13 and S14, Supporting Information).

Finally, we demonstrate that this method is not limited to aluminum chemistry by depositing zinc sulfide (ZnS) using alternating injections of a solution of diethyl zinc and a solution of hydrogen sulfide. The resulting deposition on silica spheres showed a conformal coating, without external precipitation or agglomeration (Figure 3g,n; Figure S15, Supporting Information). However, the coating featured multiple homogeneously dispersed ZnS crystallites surrounded by an amorphous phase (Figure S15, Supporting Information), leading to a rougher coating. Both the presence of a rougher coating and the presence of crystallites were systematically observed in gas-phase ALD when depositing ZnS, showing that the liquid-phase method leads to comparable results.[31–33]

To illustrate this concept for use in catalysis, a model catalyst of palladium nanoparticles supported on silica was prepared to study the ability of the overcoat to prevent nanoparticle sintering, which is a common deactivation mechanism in catalysis that has been hindered in several studies by gas-phase ALD processes.[34,35] To test the effectiveness of our method for this application, cycles of oxidation and reduction were repeated on coated (20 cycles) and uncoated catalysts. The uncoated palladium catalyst started with a relatively high quantity of accessible palladium but its dispersion decreased with each thermal treatment, which was the result of sintering (**Figure 4**a). In comparison, the coated catalyst had fewer accessible palladium sites due to overage by the overcoat (Figure 4b), but this accessibility remained unaffected by thermal treatments, indicating that sintering had been curtailed. These results were also supported by the particle size distribution after the third thermal treatment measured over 600 particles per sample (Figure 4c). By comparing protected and unprotected catalyst, the population of 2.5–5 nm particles is lower in the case of bare catalyst, and a significant number of particles above 10 nm are visible, while almost none are visible when the catalyst is protected. This particle size distribution indicates that, contrary to the protected catalyst, the bare catalyst suffered from the thermally activated merging of its nanoparticles (also visible in Figure S16, Supporting Information).

In summary, atomic layer deposition (ALD) on high-surface-area dispersed materials was performed using stoichiometrically limited injections in liquid phase, at room temperature and pressure without any gas-phase ALD apparatus. Coating qualities were maintained despite the simple conditions that were employed. We also avoided the use of any excess precursor, counter-reactants or purging fluid. Liquid-phase conditions also allowed us to perform several coating operations that are not possible in gas phase. We also demonstrated the applicability of this method to heterogeneous catalysts because this method could greatly democratize the use of ALD on dispersed materials; both at laboratory scale and, notably, for industrial catalyst preparation.

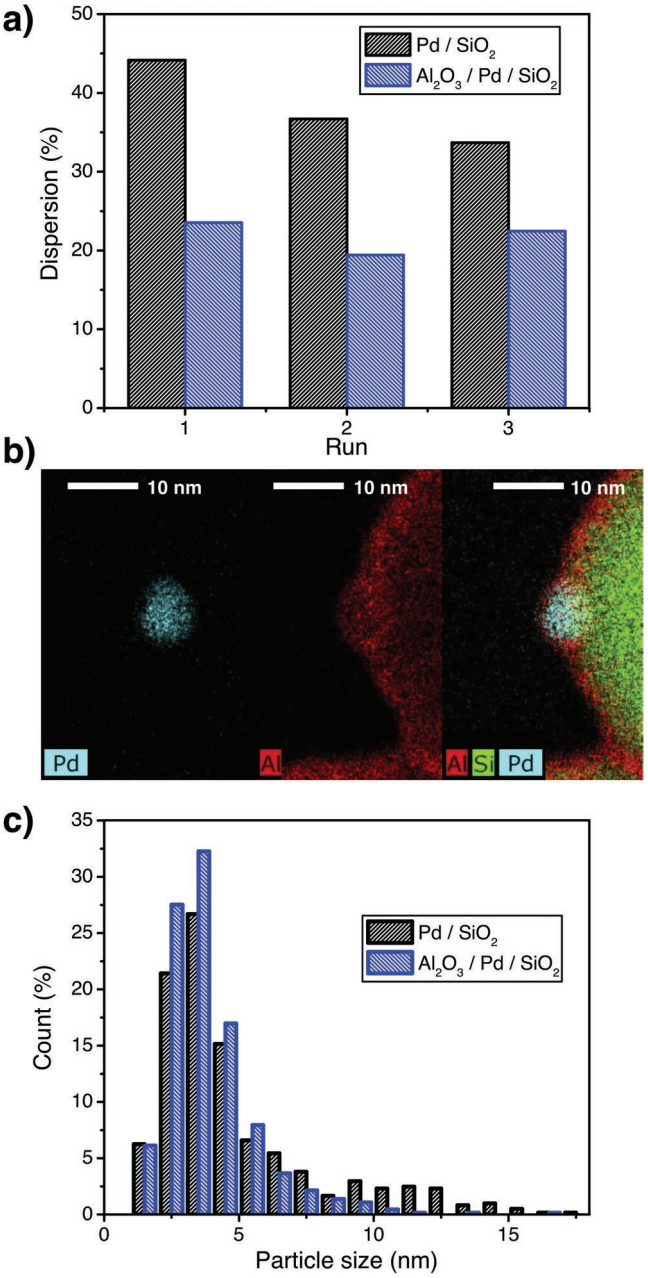

Figure 4. a) Evolution of the dispersion measured by pulse CO chemisorption and Temperature Programmed Reduction (TPR) of bare and coated Palladium catalyst during several thermal aging cycles (oxidation/reduction). b) STEM-EDX pictures of supported palladium nanoparticles on silica coated with 20 cycles of stoichiometrically injected alumina. c) Particle size distribution of both protected and unprotected catalysts, measured by TEM.

Experimental Section

All chemicals were purchased anhydrous or dried over molecular sieves (4 Å, Merck) and stored in a glovebox (typically <0.5 ppm H_2O and <5 ppm O_2). Dibutyl ether (DBE) 99+%, tetraorthosilicate (TEOS, 98%), and methyl magnesium bromide (3 M in ether) were purchased from Acros organic. Anhydrous dioxane 99.8% was purchased from ABCR. Trimethyl aluminum (TMA, 2 M in heptane), phosphoric acid, HCl (2 M in ether), diethyl zinc (1 M in heptane), and hydrogen sulfide (0.8 M in THF) were purchased from Sigma Aldrich. MgO was purchased from Fluka. High-surface-area silica was purchased from Strem. Silica spheres were prepared using a previously described method adapted from Stöber.[12,36] The density of hydroxyl groups was measured by methyl magnesium bromide titration as previously described.[37–39] The supported palladium catalyst was prepared according to a published method.[34] A short description of the methods is provided in Section S1 in the Supporting Information.

Surface titration with the precursors was performed as follows. A round bottom flask (250 mL) and a Schlenk tube (25 mL) were put in a glovebox, in which the powder, the solvent and a magnetic stirrer were loaded. A TMA solution was prepared by diluting the commercial solution into DBE using a volumetric flask. Then, the solution was transferred to the Schlenk tube. All glassware was sealed by a rubber septum and taken out of the glovebox to a fume hood equipped with a Schlenk line. The reactor was stirred for 15 min to ensure dispersion of the powder. The titration sequence consisted of the addition of the precursor solution by injection with a syringe to the stirred powder at room temperature, followed by 40 min for reaction. After this time, gas samples were taken with a gas tight syringe and injected into a GC-FID for methane quantification. The sequence was repeated until the saturation point was clearly reached. A slight increase of methane after saturation (0.01–0.3 CH_4/Al) was attributed to vapors of TMA caught by the gas syringe, which then hydrolyzed inside the GC's injector (the resulting minor slope was discounted during the determination of the saturation point, Figure S17, Supporting Information). This vapor pressure of TMA was only present when titration was carried out beyond stoichiometric saturation and thus was not present during the actual overcoating.

The same titration procedure that was used for TMA was followed for water titration, except that the water solution was prepared out of the glovebox, where typically 0.2 mL of water was added to a Schlenk tube containing 40 mL of dry dioxane. Further experimental considerations for the aluminum precursor selection, choice of solvent, and water titration are discussed in Sections S2–S4 in the Supporting Information.

Multiple liquid-phase cycles of atomic layer deposition on powders were performed by simply extending the surface titration procedure. Solutions of TMA in DBE and water in dioxane (in case of alumina deposition) were prepared in Schlenk tubes. The powder was loaded in a glovebox and the calculated volume of the precursor solution necessary to reach the stoichiometric saturation quantity measured by titration was injected at each cycle. Evacuation of the resulting methane was facilitated through a bubbler connected to a second neck of the round-bottom flask, or simply released by syringe depending on the quantity of methane expected (Figure S3, Supporting Information). For the deposition of aluminum phosphate, DBE was used to disperse the substrate and as the solvent for both the TMA and phosphoric acid injections. For experiments involving H_2S, the substrate was dispersed in DBE and solutions of diethyl zinc in heptane and H_2S in THF were used for injections. The latter procedure was carried out entirely inside a glovebox.

Fluidized bed reactor ALD (FBR-ALD) was performed using a Beneq TFS 200 instrument, the reactor chamber was set at 140 °C under reduced pressure (<1 mbar) and shaken with vibrations. Typical exposure and purge time was: 6 min TMA injection, 40 min purge, 4 min H_2O injection, 40 min purge for a single cycle with 2 g of substrate being coated.

Electron microscopy was performed on a FEI Talos with 200 keV acceleration voltage, where samples were dry impregnated on Lacey carbon grids.

Methane was systematically quantified using a Perkin Elmer Autosystem GC with a plot Q column and Flamme Ionization Detector (FID). N_2 physisorption was performed using a Micromeritics 3 flex at 77 K, where the measurement was preceded by in situ drying at 120 °C. CO titrations (at 30 °C) and TPRs (600 °C, 20 °C min^{-1}) were recorded on a Micromeritics Autochem II with a Thermal Conductivity Detector (TCD). Solid-state NMR was performed at 9.4 T on a Bruker AVIII HD spectrometer with a 2.5 mm triple-channel solid-state probe set at a spinning speed of 30 kHz recording 4096 scans. The XPS measurements were performed on a Phi Versa Probe II with an aluminum anode at

50 W. The C1s peak at 284.8 eV was used as a reference and the spectra were recorded with steps of 0.2 eV. The data were processed using CasaXPS.

Supporting Information

Supporting Information is available from the Wiley Online Library or from the author.

Acknowledgements

This work was supported by the European Research Council (ERC) under the European Union's Horizon 2020 research and innovation program (Starting grant: CATACOAT, No. 758653) and by EPFL. This work was also accomplished within the framework of the Swiss Competence Center for Bioenergy Research (SCCER-BIOSWEET). The authors also thank EPFL's interdisciplinary center for electron microscopy for support during electron microscopy measurements. The authors thank Aurelien Bornet for help with solid-state NMR measurements, Pascal Schouwink for PXRD, and Mounir Mensi for help with XPS measurements. The authors also thank Professor Kevin Sivula for useful discussions.

Conflict of Interest

The authors declare no conflict of interest.

Keywords

atomic layer deposition, nanomaterials, nanostructured catalysts, surface chemistry

Received: July 4, 2019
Revised: October 4, 2019
Published online:

[1] S. M. George, *Chem. Rev.* **2010**, *110*, 111.
[2] R. L. Puurunen, *Chem. Vap. Deposition* **2014**, *20*, 332.
[3] J. Hämäläinen, M. Ritala, M. Leskelä, *Chem. Mater.* **2014**, *26*, 786.
[4] Y.-Q. Cao, X.-R. Zhao, J. Chen, W. Zhang, M. Li, L. Zhu, X.-J. Zhang, D. Wu, A.-D. Li, *Sci. Rep.* **2018**, *8*, 12131.
[5] X. Meng, *J. Mater. Chem. A* **2017**, *5*, 18326.
[6] R. W. Johnson, A. Hultqvist, S. F. Bent, *Mater. Today* **2014**, *17*, 236.
[7] L. F. Hakim, D. M. King, Y. Zhou, C. J. Gump, S. M. George, A. W. Weimer, *Adv. Funct. Mater.* **2007**, *17*, 3175.
[8] J. Lu, J. W. Elam, P. C. Stair, *Surf. Sci. Rep.* **2016**, *71*, 410.
[9] S. Adhikari, S. Selvaraj, D.-H. Kim, *Adv. Mater. Interfaces* **2018**, *5*, 1800581.
[10] T. M. Onn, R. Küngas, P. Fornasiero, K. Huang, R. J. Gorte, *Inorganics* **2018**, *6*, 34.
[11] F. Héroguel, L. Silvioli, Y.-P. Du, J. S. Luterbacher, *J. Catal.* **2018**, *358*, 50.
[12] Y.-P. Du, F. Héroguel, J. S. Luterbacher, *Small* **2018**, *14*, 1801733.
[13] A. Loiudice, M. Strach, S. Saris, D. Chernyshov, R. Buonsanti, *J. Am. Chem. Soc.* **2019**, *141*, 8254.
[14] F. Héroguel, B. P. Le Monnier, K. S. Brown, J. C. Siu, J. S. Luterbacher, *Appl. Catal., B* **2017**, *218*, 643.
[15] K. S. Brown, C. Saggese, B. P. Le Monnier, F. Héroguel, J. S. Luterbacher, *J. Phys. Chem. C* **2018**, *122*, 6713.
[16] H. M. Pathan, C. D. Lokhande, *Bull. Mater. Sci.* **2004**, *27*, 85.
[17] Y. Wu, D. Döhler, M. Barr, E. Oks, M. Wolf, L. Santinacci, J. Bachmann, *Nano Lett.* **2015**, *15*, 6379.
[18] R. L. Puurunen, *J. Appl. Phys.* **2005**, *97*, 121301.
[19] J. Li, J. A. DiVerdi, G. E. Maciel, *J. Am. Chem. Soc.* **2006**, *128*, 17093.
[20] R. N. Kerber, A. Kermagoret, E. Callens, P. Florian, D. Massiot, A. Lesage, C. Copéret, F. Delbecq, X. Rozanska, P. Sautet, *J. Am. Chem. Soc.* **2012**, *134*, 6767.
[21] C. Guerra-Nuñez, M. Döebeli, J. Michler, I. Utke, *Chem. Mater.* **2017**, *29*, 8690.
[22] A. C. Dillon, A. W. Ott, J. D. Way, S. M. George, *Surf. Sci.* **1995**, *322*, 230.
[23] J. A. McCormick, K. P. Rice, D. F. Paul, A. W. Weimer, S. M. George, *Chem. Vap. Deposition* **2007**, *13*, 491.
[24] M. B. M. Mousa, C. J. Oldham, G. N. Parsons, *Langmuir* **2014**, *30*, 3741.
[25] M. D. Groner, F. H. Fabreguette, J. W. Elam, S. M. George, *Chem. Mater.* **2004**, *16*, 639.
[26] R. L. Puurunen, W. Vandervorst, *J. Appl. Phys.* **2004**, *96*, 7686.
[27] L. T. Zhuravlev, *Colloids Surf. A* **2000**, *173*, 1.
[28] J. Hämäläinen, J. Holopainen, F. Munnik, M. Heikkilä, M. Ritala, M. Leskelä, *J. Phys. Chem. C* **2012**, *116*, 5920.
[29] M. K. Wiedmann, D. H. K. Jackson, Y. J. Pagan-Torres, E. Cho, J. A. Dumesic, T. F. Kuech, *J. Vac. Sci. Technol., A* **2012**, *30*, 01A134.
[30] S. Knohl, A. K. Roy, R. Lungwitz, S. Spange, T. Mäder, D. J. Nestler, B. Wielage, S. Schulze, M. Hietschold, H. Wulff, C. A. Helm, F. Seidel, D. R. T. Zahn, W. A. Goedel, *ACS Appl. Mater. Interfaces* **2013**, *5*, 6161.
[31] Y. S. Kim, S. J. Yun, *Appl. Surf. Sci.* **2004**, *229*, 105.
[32] J. Ihanus, M. Ritala, M. Leskelä, T. Prohaska, R. Resch, G. Friedbacher, M. Grasserbauer, *Appl. Surf. Sci.* **1997**, *120*, 43.
[33] R. J. Ding, L. He, Z. Ye, A. L. Cui, C. H. Sun, L. F. Liu, X. N. Hu, in *Infrared Technology Applications XLIV* (Eds: B. F. Andresen, G. F. Fulop, C. M. Hanson, P. R. Norton, B. F. Andresen, J. L. Miller), SPIE, Bellingham, WA, USA **2018**, p. 72.
[34] J. Lu, B. Fu, M. C. Kung, G. Xiao, J. W. Elam, H. H. Kung, P. C. Stair, *Science* **2012**, *335*, 1205.
[35] B. J. O'Neill, D. H. K. Jackson, A. J. Crisci, C. A. Farberow, F. Shi, A. C. Alba-Rubio, J. Lu, P. J. Dietrich, X. Gu, C. L. Marshall, P. C. Stair, J. W. Elam, J. T. Miller, F. H. Ribeiro, P. M. Voyles, J. Greeley, M. Mavrikakis, S. L. Scott, T. F. Kuech, J. A. Dumesic, *Angew. Chem.* **2013**, *125*, 14053.
[36] W. Stöber, A. Fink, E. Bohn, *J. Colloid Interface Sci.* **1968**, *26*, 62.
[37] F. Qi, B. Xu, Z. Chen, L. Zhang, P. Zhang, D. Sun, *Chem. Eng. J.* **2010**, *165*, 490.
[38] F. Qi, Z. Chen, B. Xu, J. Shen, J. Ma, C. Joll, A. Heitz, *Appl. Catal., B* **2008**, *84*, 684.
[39] H. Tamura, A. Tanaka, K. Mita, R. Furuichi, *J. Colloid Interface Sci.* **1999**, *209*, 225.